

# Rotational Multiplexing Method Based on Cascaded Metasurface Holography

Qunshuo Wei, Lingling Huang,\* Ruizhe Zhao, Guangzhou Geng, Junjie Li, Xiaowei Li, and Yongtian Wang

Since the emergence of optical metasurfaces, their outstanding wavefront modulation ability and numerous degrees of freedom (DOFs) have motivated many multiplexing methods, and many unprecedented functionalities and impressive advances have been achieved. However, the number of DOFs of single-layer metasurfaces is intrinsically limited. To further explore the innovative multiplexing dimensions and application scenarios of metasurfaces, multilayer and cascaded metasurfaces are proposed. Inspired by the alignment sensitivity of cascaded metasurface holography, here the authors use the in-plane rotation between two cascaded metasurfaces as an additional design DOF to introduce the concept of the rotational multiplexing method. An iterative gradient optimization scheme based on a machine learning method is developed to obtain the phase profiles. Dual working modes can be achieved, and both single-layer and rotational cascaded holography can be reconstructed in the far-field. Such versatile configurations may provide promising solutions for optical encryption, data storage, and dynamic display.

of metasurfaces stem from the large variety of possible geometric shapes, structural sizes, spatial orientation angles, combination modes, and wavefront modulation mechanisms. Owing to their unique abilities to modulate the arbitrary phase, amplitude, polarization, wavelength, and orbital angular momentum of light, metasurfaces produce various special optical effects, which lead to a multitude of potential applications such as holography,<sup>[5–8]</sup> color printing,<sup>[9–11]</sup> beam shaping,<sup>[12]</sup> edge detection,<sup>[13]</sup> generation and measurement of polarization,<sup>[14,15]</sup> generation and manipulation of THz waves,<sup>[16]</sup> and optical encryption and anticounterfeiting.<sup>[17,18]</sup>

To increase the information capacity of metasurfaces and fully utilize the excellent wavefront modulation ability and numerous DOFs of metasurfaces, several multiplexing methods have been proposed

## 1. Introduction

Metasurfaces composed of 2D arrangements of plasmonic or dielectric nanoantennas have attracted enormous interest owing to their ability to enable high degrees of freedom (DOFs) to tailor the optical properties of light with ultra-thin thicknesses.<sup>[1–4]</sup> The powerful versatility and great design flexibility

that utilize fundamental light properties or spatial arrangements, such as spatial multiplexing,<sup>[19]</sup> polarization multiplexing,<sup>[20–22]</sup> angular multiplexing,<sup>[23,24]</sup> orbital angular momentum multiplexing,<sup>[25,26]</sup> spectral and spatial multiplexing,<sup>[27,28]</sup> near- and far-field multiplexing,<sup>[29,30]</sup> and nonlinear wavelength multiplexing.<sup>[31]</sup> For example, a coherent pixel was proposed based on the coherent superposition of electromagnetic fields, which can be used to obtain angle-multiplexed scalar or switchable vectorial print images.<sup>[32,33]</sup> Detour phase holograms combined with spatial multiplexing can record four independent phase profiles with respect to the incident angles using a single metasurface device.<sup>[34]</sup> Moreover, with a single-cell design approach that manipulates the spectrum, polarization, and phase of incident light, a tri-functional metasurface that can act as a color printing image, polarization-controlled grayscale image, and hologram was demonstrated.<sup>[35]</sup> Furthermore, by exploiting the constructive and destructive interference between hybrid meta-atoms, an interference-assisted metasurface multiplexer was achieved.<sup>[36]</sup> The above methods achieved many advanced functionalities and have paved the way for broader exploitation of metasurfaces. However, for a single-layer metasurface, the number of DOFs is intrinsically limited owing to its mirror symmetry with respect to its structural plane.<sup>[37]</sup> On the other hand, single-layer solutions only provide different information channels for multiplexing and cannot physically split information.

Recently, multilayer metasurfaces and cascaded metasurfaces have been developed rapidly and have achieved many previously

Q. Wei, L. Huang, R. Zhao, Y. Wang  
Beijing Engineering Research Center of Mixed Reality  
and Advanced Display  
School of Optics and Photonics  
Beijing Institute of Technology  
Beijing 100081, China  
E-mail: huanglingling@bit.edu.cn

G. Geng, J. Li  
Beijing National Laboratory for Condensed Matter Physics  
Institute of Physics  
Chinese Academy of Sciences  
Beijing 100190, China

X. Li  
Laser Micro/Nano-Fabrication Laboratory  
School of Mechanical Engineering  
Beijing Institute of Technology  
Beijing 100081, China

 The ORCID identification number(s) for the author(s) of this article can be found under <https://doi.org/10.1002/adom.202102166>.

DOI: 10.1002/adom.202102166

unrealized functionalities. Integrated multilayer metasurface layouts have often been used to achieve kaleidoscopic wavefront control,<sup>[38]</sup> multispectral achromatic metalenses,<sup>[39]</sup> image differentiation,<sup>[40]</sup> Janus metasurfaces with bidirectional functionality,<sup>[41–43]</sup> holography with asymmetric transmission,<sup>[44]</sup> holography with color printing,<sup>[45]</sup> and all-optical machine learning frameworks.<sup>[46]</sup> For cascaded metasurfaces, whose components can be replaced, translated, or rotated, impressive functionalities such as prescribing light trajectories,<sup>[47]</sup> Moiré metalens for adjustable focal length,<sup>[48]</sup> dynamical wavefront modulators,<sup>[49]</sup> etc., have been demonstrated. Furthermore, the cascaded holography method allows for physical separation and combination of encoded information. By separating the designed phase profile into two matrices, a reprogrammable metasurface that can produce arbitrary holographic images for optical encryption via illumination with a spatial light modulator was proposed.<sup>[50]</sup> In particular, an all-optical solution for secret sharing based on cascaded metasurface holography has been demonstrated.<sup>[51]</sup> All the single metasurface holograms and cascaded configurations can create an independent holographic image.

In this study, inspired by the inherent sensitivity in the translational and longitudinal alignment manipulation of cascaded metasurface holography,<sup>[52]</sup> we further utilize the in-plane rotation angle as an additional design DOF to introduce the concept of the rotational multiplexing method. Different relative in-plane rotation between two stacked metasurface holograms correspond to completely different cascaded metasurface systems. In our design, such a cascade metasurface system consists of two Fourier metasurface holograms, each of which can reconstruct a distinct holographic image in the far-field. Four independent new holographic images can be observed when these two metasurface holograms are stacked together with different relative in-plane rotations of 0°, 90°, 180°, and 270°. In other words, reconstructed images can be switched by rotating one of the metasurface holograms around the normal at its geometric center. To achieve this, we used an iterative gradient optimization scheme with the help of a machine learning method. This method can make full use of the in-plane rotation angle as a design DOF, provide an innovative holographic security feature, and offer a novel perspective for improving the information capacity and design flexibility of metasurfaces. As a platform for data storage and optical encryption, our rotational multiplexing cascaded metasurface holography is expected to be a potential candidate that plays a key role in related fields.

## 2. Results

As a proof of concept, we designed and fabricated two geometric phase metasurfaces to experimentally demonstrate our method under circularly polarized light illumination. **Figure 1** schematically illustrates the dual working modes of the proposed rotational multiplexing cascaded metasurfaces. In the single-layer mode, each metasurface hologram has its own target image. On the other hand, for the cascaded mode, the two metasurface holograms are stacked together, where the light passing through the cascaded metasurfaces accumulates the phase delays of both layers. Therefore, four cascaded configurations that correspond to four specific relative in-plane

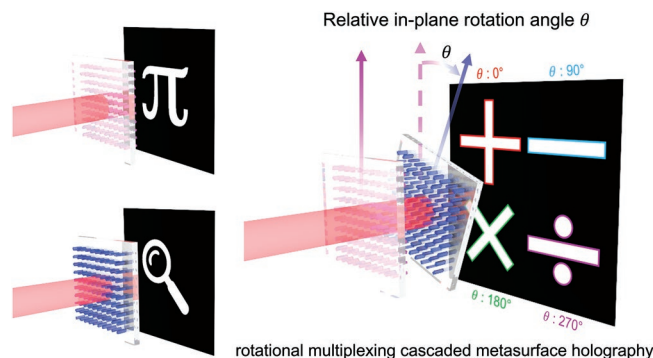


**Figure 1.** Schematic illustration of the rotational multiplexing cascaded metasurfaces. A total of six different holographic images can be reconstructed upon the single-layer mode and the cascaded mode.

rotation angles ( $\theta$ ) between the two metasurface holograms can be regarded as completely different systems, which result in four new holographic images distinct from each single-layer metasurface hologram. Therefore, a total of six different holographic images can be obtained through two metasurfaces.

To design and optimize the shape and period of the metaatoms, we used a rigorous coupled-wave analysis simulation method. We chose amorphous silicon ( $\alpha$ -Si) nanofins as building blocks to construct our geometric phase metasurfaces, which behave as local half-wave plates and maximize circular cross-polarization conversion transmittance. Considering the balance of fabrication accuracy and broadband property, we chose a 600 nm height nanofin with a length of 195 nm and a width of 130 nm for our geometric phase metasurface, with a period of 500 nm in both the x- and y-directions (see part A of Supporting Information for details). According to the geometric phase modulation mechanism, each nanofin induces an azimuthal-angle-dependent local abrupt phase change, which occurs for circularly polarized light when converted to its opposite helicity. The broadband and polarization selective characteristics of the geometric phase offer the advantage of being quite robust with regard to fabrication and allow for filtering unwanted light. We fabricated two distinct metasurface holograms on two glass substrates following silicon deposition, patterning, lift-off, and etching. Details regarding the design and fabrication can be found in the Supporting Information.

The design algorithm for the phase profiles of holograms plays an important role in cascaded rotational multiplexing method. To endow our cascaded metasurfaces with the powerful function of rotational multiplexing, we introduced a gradient optimization scheme that treats the design process as an optimization problem. Such gradient optimization scheme consists of two different parts: the explicit formulations of the forward calculation and the use of a gradient optimizer. The ultimate purpose of this scheme is to minimize the mean squared error (MSE) between the target images and calculated images resulting from the simulated light propagation process. As shown in **Figure 2**, the design flowchart for the gradient optimization scheme is as follows. First, we need to calculate the total error function which benchmarks the overall holographic reconstruction quality of the phase profiles. For the single-layer mode, two metasurface holograms correspond to two

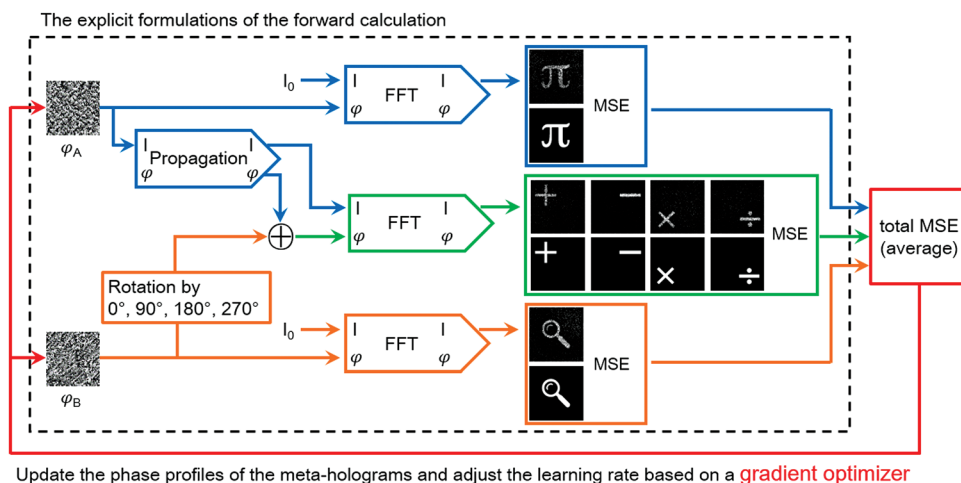


**Figure 2.** The flowchart of the gradient optimization scheme that endows the cascaded metasurfaces with the function of rotational multiplexing. The gradient optimization scheme consists of two different parts: the explicit formulations of the forward calculation as well as the usage of a gradient optimizer.

arbitrary phase profiles,  $\phi_A$  and  $\phi_B$ . For the cascaded mode, for example, if we keep phase profile  $\phi_A$  and rotate phase profile  $\phi_B$  by in-plane rotations of  $0^\circ$ ,  $90^\circ$ ,  $180^\circ$ , and  $270^\circ$ , four different phase profiles corresponding to four cascaded configurations can be obtained. For the light propagation between the two metasurfaces in the cascaded case, we use the angular spectrum method with zero padding for the simulation. We perform a fast Fourier transformation for all six-phase profiles to obtain the reconstruction results of all six holographic images, and then compare them with the target images by using the MSE. The total MSE  $\alpha$  is defined as the average of the MSEs with regard to all six holographic images. Second, the gradient  $\nabla\alpha(\phi)$  is defined as the derivative of the total MSE  $\alpha$ . Finally, we use a gradient optimizer based on Adam, which updates the phase profiles based on the current learning rate in each iteration and adjusts the learning rate during the optimization to converge the gradient  $\nabla\alpha(\phi)$  toward a local optimum. Additionally, we modify the learning rate according to the comparison result. Our developed algorithmic approach provides an efficient and straightforward approach to design the phase profiles for rotational multiplexing cascaded metasurfaces.

We demonstrated the functionality and performance of such rotational multiplexing cascaded metasurfaces using the experimental setup shown in **Figure 3a**. Considering the properties of the geometric phase modulation mechanism, a linear polarizer, and quarter-wave plate were positioned in front of as well as afterward the metasurface holograms as circular polarizers to prepare and select the desired circular polarization state for the incident/transmitted light (cross-polarized light for the single-layer mode, co-polarized light for the cascaded mode). The two metasurfaces were placed on two 3D translation tables, and the distance between them was set to  $100\ \mu\text{m}$ . All holographic images appeared in k-space. A lens with a focal length of  $150\ \text{mm}$  was used to observe the Fourier plane on the CCD camera. For the cascaded mode, a  $40\times$  magnifying microscope objective was positioned behind the stacked metasurface holograms for precise pixel alignment.

A high alignment sensitivity with regard to in-plane translation and rotation was anticipated and confirmed in advance (see part C of Supporting Information for details). Therefore, we intentionally fabricated a pixel size larger than the intrinsic metasurface resolution by repeatedly placing nanofins with the same azimuthal angle. The size of the metasurface holograms was  $496 \times 496\ \mu\text{m}^2$ , containing  $62 \times 62$  pixels with a side length of  $8\ \mu\text{m}$ . Two exemplary scanning electron microscopy (SEM) images of the samples in the top and side views are shown in **Figure 3b**.

**Figure 4** shows the experimentally reconstructed holographic images of the single-layer mode and the cascaded mode of rotational multiplexing. As shown in **Figure 4a**, when illuminated by circularly polarized light with a wavelength of  $800\ \text{nm}$ , both single-layer metasurface holograms yield their target holographic images of a symbol “ $\pi$ ” and a magnifier, with satisfactory quality and low background noise at far-field, respectively. For the cascaded mode, as marked by white dotted boxes in **Figure 4b**, four distinct reconstructed holographic images of

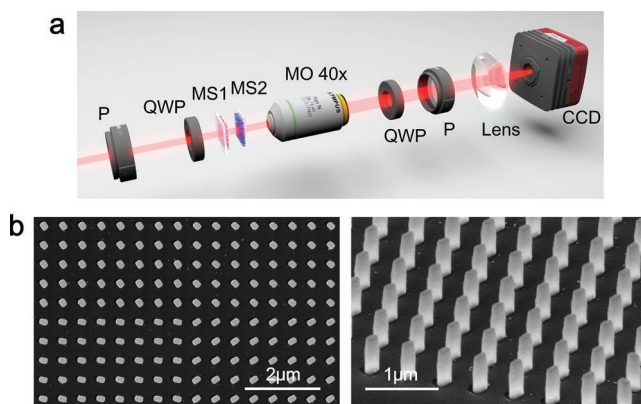


**Figure 3.** The experimental setup and the SEM images of the metasurface holograms. a) Schematic of the experimental setup for observing the holographic images. P: linear polarizer, QWP: quarter waveplate, MS: metasurface, MO: microscope objective. b) The SEM images of the metasurface holograms in top and side view, respectively.

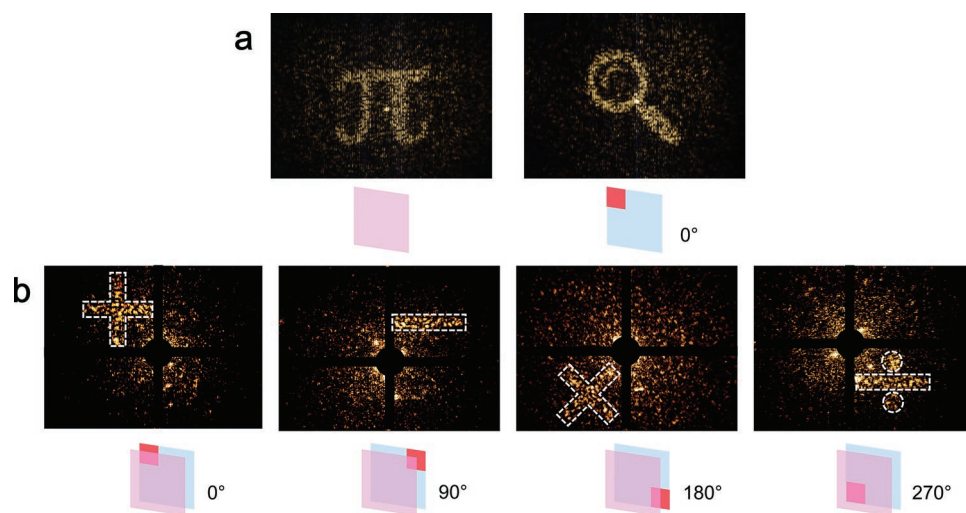


**Figure 4.** The experimental reconstructed holographic images of the dual working modes. a) Single-layer mode. b) Cascaded mode with rotational multiplexing. As marked by white dotted boxes, four distinct reconstructed holographic images of the symbols “+”, “-”, “x” and “+” can be observed when two metasurface holograms are stacked together along the propagation direction and their relative in-plane rotation angles are  $0^\circ$ ,  $90^\circ$ ,  $180^\circ$ , and  $270^\circ$ , respectively.

the symbols “+”, “-”, “x”, and “+” can be observed when two metasurface holograms are stacked together along the propagation direction and their relative in-plane rotation angles are  $0^\circ$ ,  $90^\circ$ ,  $180^\circ$ , and  $270^\circ$ , respectively. Compared with their single-layer counterparts, the reconstruction qualities of holographic images in the cascaded mode are relatively lower for several reasons. First, the nanofins may deviate from the designed ones owing to fabrication defects as well as small deviations in the refractive index of amorphous silicon. Such cascaded metasurfaces superimpose the potential fabrication errors of the two metasurfaces, resulting in the accumulation of extra phase noise. Second, for the cascaded mode, circularly polarized light passes through two geometric metasurfaces in turn, and its polarization should ideally be converted back and forth. Hence, we measured circularly polarized light with the same helicity as the incident light in our experiment. Under these conditions, some residual light passes through both metasurfaces without changing its circular polarization state, which leads to a zeroth-order spot that cannot be filtered by polarization selection.

### 3. Conclusion

Such rotational multiplexing cascaded metasurfaces can be further extended by combining them with established metasurface polarization multiplexing concepts. A polarization-multiplexing metasurface essentially carries two or more different phase profiles, which can be selected according to the choice of polarization. Thus, two or more arbitrary target images can be encoded within a single cascaded configuration, which offers twice or more information capacity for the cascaded mode. In addition, to make full use of the in-plane rotation angle as a design DOF, one can design a round metasurface and further increase the number of cascaded configurations through rotation. Furthermore, our method is scalable in terms of the number of stacked metasurfaces and the combinatorial cascading of two sets of metasurfaces.

In summary, it is worth noting that the inherent alignment sensitivity between two stacked metasurface holograms can be utilized to store additional information with different configurations. In this study, we explore in-plane rotation as a novel multiplexing dimension and introduce an effective algorithm for achieving cascaded metasurface holography. Six different holographic images were successfully demonstrated experimentally in single-layer and cascaded modes. Owing to its large information capacity, strong controllability, and dual-mode design, our method has huge potential for optical encryption and anticounterfeiting with a high security level and opens new possibilities for the frontier research of high-density image storage, optical information processing, dynamic display, and many other fields.

### 4. Experimental Section

**Fabrication of the Metasurfaces:** The authors fabricated cascaded metasurfaces on two fused quartz substrates using electron beam lithography following the processes of deposition, patterning, lift-off, and etching. First, a 600-nm-thick amorphous silicon ( $\alpha$ -Si) film was deposited using plasma-enhanced chemical vapor deposition (PECVD). Subsequently, a PMMA film with a thickness of 300 nm was spin-coated and covered by a PEDOT:PSS film as a conducting layer. The desired structures were patterned using standard electron beam lithography. After the exposure process, the conducting layer was washed away and the resist was developed in a 1:3 MIBK:IPA solution and rinsed in IPA successively, followed by the deposition of 80 nm Cr using the electron beam evaporation deposition method. To realize the lift-off process, the sample was immersed in hot acetone at  $75^\circ\text{C}$  and ultrasonically cleaned. Finally, using the inductively coupled plasma reactive ion etching (ICP-RIE) method, the desired structures were transferred from Cr to silicon, and the residual Cr was removed by cerium (IV) ammonium nitrate.

**The Gradient Optimization Scheme:** To endow the cascaded metasurfaces with the function of rotational multiplexing, a gradient optimization scheme was introduced that treats the design process as an optimization problem. For gradient optimizers in the machine learning field, the choice of the hyperparameter “learning rate”, which

scales the step size in the optimization process, heavily determines the speed and accuracy of convergence. If the learning rate was set too high, the optimization scheme does not converge at all, and if the learning rate was set too low, the convergence becomes very slow. To make the optimization process resilient, an Adam-based gradient optimizer was introduced to adjust the learning rate per iteration.

Specifically, for a given phase profile set, such a gradient optimizer suggests new phase profiles based on the current learning rate for each iteration. However, instead of simply choosing this new phase profile and repeating the iteration process, the authors obtain another new phase profile based on the current learning rate by taking the same step once more and performing a second evaluation. The authors then compare the initial phase profile set with the two new candidates and choose the one with the lowest error. In addition, the learning rate was modified according to the comparison results. The authors slow down when a local minimum was overshoot, and otherwise was accelerated. Therefore, such a gradient optimizer can accelerate the convergence speed and guarantee convergence towards a local optimum.

## Supporting Information

Supporting Information is available from the Wiley Online Library or from the author.

## Acknowledgements

The authors acknowledge the funding provided by the Beijing Outstanding Young Scientist Program (BJJWZYJH01201910007022), the National Natural Science Foundation of China (No. 61775019, No. 92050117, No. 61861136010), the Beijing Municipal Science and Technology Commission, Administrative Commission of Zhongguancun Science Park (No. Z211100004821009), and the Fok Ying-Tong Education Foundation of China (No. 161009).

## Conflict of Interest

The authors declare no conflict of interest.

## Author Contributions

Q.W. and L.H. conceived the idea for this work. Q.W. conducted the structure design, numerical simulations, and hologram generations; G.G. and J.L. fabricated the samples; Q.W. and R.Z. performed the measurements; Q.W. and L.H. prepared the manuscript. L.H., X.L., and Y.W. supervised the project. All authors analyzed the data and discussed the results.

## Data Availability Statement

The data that support the findings of this study are available from the corresponding author upon reasonable request.

## Keywords

cascaded metasurfaces, holography, optical encryption, rotational multiplexing

Received: October 10, 2021

Revised: January 11, 2022

Published online:

- [1] H. Hsiao, H. Cheng, D. Tsai, *Small Methods* **2017**, *1*, 1600064.
- [2] F. Ding, A. Pors, S. I. Bozhevolnyi, *Rep. Prog. Phys.* **2018**, *81*, 026401.
- [3] J. Sung, G. Lee, B. Lee, *Nanophotonics* **2019**, *8*, 1701.
- [4] P. Genevet, F. Capasso, F. Aieta, M. Khorasaninejad, R. Devlin, *Optica* **2017**, *4*, 139.
- [5] X. Li, R. Zhao, Q. Wei, G. Geng, J. Li, S. Zhang, L. Huang, Y. Wang, *Adv. Funct. Mater.* **2021**, *31*, 2103326.
- [6] Y. Bao, J. Yan, X. Yang, C. Qiu, B. Li, *Nano Lett.* **2021**, *21*, 2332.
- [7] B. Xiong, Y. Xu, J. Wang, L. Li, L. Deng, F. Cheng, R. Peng, M. Wang, Y. Liu, *Adv. Mater.* **2021**, *33*, 2005864.
- [8] R. Zhao, L. Huang, Y. Wang, *PhotonIX* **2020**, *1*, 20.
- [9] W. Yang, S. Xiao, Q. Song, Y. Liu, Y. Wu, S. Wang, J. Yu, J. Han, D. Tsai, *Nat. Commun.* **2020**, *11*, 1864.
- [10] X. Duan, S. Kamin, N. Liu, *Nat. Commun.* **2017**, *8*, 14606.
- [11] Z. Dong, J. Ho, Y. F. Yu, Y. H. Fu, R. Paniagua-Dominguez, S. Wang, A. I. Kuznetsov, J. K. W. Yang, *Nano Lett.* **2017**, *17*, 7620.
- [12] Z. Lin, X. Li, R. Zhao, X. Song, Y. Wang, L. Huang, *Nanophotonics* **2019**, *8*, 1079.
- [13] A. Komar, R. A. Aoni, L. Xu, M. Rahmani, A. E. Miroshnichenko, D. N. Neshev, *ACS Photonics* **2021**, *8*, 864.
- [14] Y. Xu, Q. Li, X. Zhang, M. Wei, Q. Xu, Q. Wang, H. Zhang, W. Zhang, C. Hu, Z. Zhang, C. Zhang, X. Zhang, J. Han, W. Zhang, *ACS Photonics* **2019**, *6*, 2933.
- [15] X. Zhang, S. Yang, W. Yue, Q. Xu, C. Tian, X. Zhang, E. Plum, S. Zhang, J. Han, W. Zhang, *Optica* **2019**, *6*, 1190.
- [16] Y. Lu, X. Feng, Q. Wang, X. Zhang, M. Fang, W. Sha, Z. Huang, Q. Xu, L. Niu, X. Chen, C. Ouyang, Y. Yang, X. Zhang, E. Plum, S. Zhang, J. Han, W. Zhang, *Nano Lett.* **2021**, *21*, 7699.
- [17] L. Jin, Z. Dong, S. Mei, Y. F. Yu, Z. Wei, Z. Pan, S. D. Rezaei, X. Li, A. I. Kuznetsov, Y. S. Kivshar, J. K. W. Yang, C. Qiu, *Nano Lett.* **2018**, *18*, 8016.
- [18] H. Liu, B. Yang, Q. Guo, J. Shi, C. Guan, G. Zheng, H. Mühlenbernd, G. Li, T. Zentgraf, S. Zhang, *Sci. Adv.* **2017**, *3*, e1701477.
- [19] B. Wang, F. Dong, Q. Li, D. Yang, C. Sun, J. Chen, Z. Song, L. Xu, W. Chu, Y. Xiao, Q. Gong, Y. Li, *Nano Lett.* **2016**, *16*, 5235.
- [20] Z. Deng, M. Jin, X. Ye, S. Wang, T. Shi, J. Deng, N. Mao, Y. Cao, B. Guan, A. Alu, G. Li, X. Li, *Adv. Funct. Mater.* **2020**, *30*, 1910610.
- [21] R. Zhao, B. Sain, Q. Wei, C. Tang, X. Li, T. Weiss, L. Huang, Y. Wang, T. Zentgraf, *Light: Sci. Appl.* **2018**, *7*, 95.
- [22] E. Arbabi, S. M. Kamali, A. Arbabi, A. Faraon, *ACS Photonics* **2019**, *6*, 2712.
- [23] S. M. Kamali, E. Arbabi, A. Arbabi, Y. Horie, M. Faraji-Dana, A. Faraon, *Phys. Rev. X* **2017**, *7*, 41056.
- [24] C. Spägle, M. Tamagnone, D. Kazakov, M. Ossiander, M. Piccardo, F. Capasso, *Nat. Commun.* **2021**, *12*, 3787.
- [25] H. Ren, X. Fang, J. Jang, J. Bürger, J. Rho, S. A. Maier, *Nat. Nanotechnol.* **2020**, *15*, 948.
- [26] H. Zhou, B. Sain, Y. Wang, C. Schlickriede, R. Zhao, X. Zhang, Q. Wei, X. Li, L. Huang, T. Zentgraf, *ACS Nano* **2020**, *14*, 5553.
- [27] Y. Bao, Y. Yu, H. Xu, C. Guo, J. Li, S. Sun, Z. Zhou, C. Qiu, X. Wang, *Light: Sci. Appl.* **2019**, *8*, 95.
- [28] Q. Wei, B. Sain, Y. Wang, B. Reineke, X. Li, L. Huang, T. Zentgraf, *Nano Lett.* **2019**, *19*, 8964.
- [29] J. Li, Y. Wang, C. Chen, R. Fu, Z. Zhou, Z. Li, G. Zheng, S. Yu, C. Qiu, S. Zhang, *Adv. Mater.* **2021**, *33*, 2007507.
- [30] R. Zhao, X. Xiao, G. Geng, X. Li, J. Li, X. Li, Y. Wang, L. Huang, *Adv. Funct. Mater.* **2021**, *31*, 2100406.
- [31] D. Frese, Q. Wei, Y. Wang, M. Cinchetti, L. Huang, T. Zentgraf, *ACS Photonics* **2021**, *8*, 1013.
- [32] Y. Bao, Y. Yu, H. Xu, Q. Lin, Y. Wang, J. Li, Z. Zhou, X. Wang, *Adv. Funct. Mater.* **2018**, *28*, 1805306.
- [33] E. Wang, J. Niu, Y. Liang, H. Li, Y. Hua, L. Shi, C. Xie, *Adv. Opt. Mater.* **2020**, *8*, 1901674.
- [34] J. Jang, G. Lee, J. Sung, B. Lee, *Adv. Opt. Mater.* **2021**, *9*, 2100678.

- [35] Q. Dai, Z. Guan, S. Chang, L. Deng, J. Tao, Z. Li, Z. Li, S. Yu, G. Zheng, S. Zhang, *Adv. Funct. Mater.* **2020**, *30*, 2003990.
- [36] H. Xu, G. Hu, Y. Li, L. Han, J. Zhao, Y. Sun, F. Yuan, G. Wang, Z. Jiang, X. Li, T. Cui, C. Qiu, *Light: Sci. Appl.* **2019**, *8*, 3.
- [37] Y. Bao, L. Wen, Q. Chen, C. Qiu, B. Li, *Sci. Adv.* **2021**, *7*, h365.
- [38] H. Xu, G. Hu, M. Jiang, S. Tang, Y. Wang, C. Wang, Y. Huang, X. Ling, H. Liu, J. Zhou, *Adv. Mater. Technol.* **2019**, *5*, 1900710.
- [39] Y. Zhou, I. I. Kravchenko, H. Wang, J. R. Nolen, G. Gu, J. Valentine, *Nano Lett.* **2018**, *18*, 7529.
- [40] Y. Zhou, H. Zheng, I. I. Kravchenko, J. Valentine, *Nat. Photonics* **2020**, *14*, 316.
- [41] Y. Chen, X. Yang, J. Gao, *Light: Sci. Appl.* **2019**, *8*, 45.
- [42] K. Chen, G. Ding, G. Hu, Z. Jin, J. Zhao, Y. Feng, T. Jiang, A. Alu, C. Qiu, *Adv. Mater.* **2020**, *32*, 1906352.
- [43] H. Xu, C. Wang, G. Hu, Y. Wang, S. Tang, Y. Huang, X. Ling, W. Huang, C. Qiu, *Adv. Opt. Mater.* **2021**, *9*, 2100190.
- [44] D. Frese, Q. Wei, Y. Wang, L. Huang, T. Zentgraf, *Nano Lett.* **2019**, *19*, 3976.
- [45] Y. Hu, X. Luo, Y. Chen, Q. Liu, X. Li, Y. Wang, N. Liu, H. Duan, *Light: Sci. Appl.* **2019**, *8*, 86.
- [46] X. Lin, Y. Rivenson, N. T. Yardimej, M. Veli, Y. Luo, M. Jarrahi, A. Ozcan, *Science* **2018**, *361*, 1004.
- [47] A. McClung, M. Mansouree, A. Arbabi, *Light: Sci. Appl.* **2020**, *9*, 93.
- [48] Y. Luo, C. H. Chu, S. Vyas, H. Y. Kuo, Y. H. Chia, M. K. Chen, X. Shi, T. Tanaka, H. Misawa, Y. Huang, D. P. Tsai, *Nano Lett.* **2021**, *21*, 5133.
- [49] X. Cai, R. Tang, H. Zhou, Q. Li, S. Ma, D. Wang, T. Liu, X. Ling, W. Tan, Q. He, S. Xiao, L. Zhou, *Adv. Photonics* **2021**, *3*, 36003.
- [50] G. Qu, W. Yang, Q. Song, Y. Liu, C. Qiu, J. Han, D. Tsai, S. Xiao, *Nat. Commun.* **2020**, *11*, 5484.
- [51] P. Georgi, Q. Wei, B. Sain, C. Schlickriede, Y. Wang, L. Huang, T. Zentgraf, *Sci. Adv.* **2021**, *7*, f9718.
- [52] J. Jang, T. Badloe, J. Rho, *Light: Sci. Appl.* **2021**, *10*, 144.